Annealing-induced extension of the antiferromagnetic phase in epitaxial terbium metal films

F. Heigl,* J. E. Prieto, O. Krupin, K. Starke,† and G. Kaindl
Institut für Experimentalphysik, Freie Universität Berlin, Arnimallee 14, D-14195 Berlin, Germany

M. Bode
Institut für Angewandte Physik, Universität Hamburg, Jungiusstrasse 11, D-20355 Hamburg, Germany
(Received 17 December 2004; revised manuscript received 18 April 2005; published 6 July 2005)

The temperature range of helical antiferromagnetic (AFM) order in epitaxially grown Tb metal films on W(110) was studied via ac susceptibility using the magneto-optical Kerr effect. The temperature range of the AFM phase was found to get wider with increasing annealing temperature, reaching a maximum width of 17 K when the film is annealed at $T_{an}=1200$ K. This shows that the AFM phase is stabilized in epitaxial films as compared to bulk Tb metal. Annealing-induced changes of the surface topography of the films were monitored by scanning tunnel microscope and low-eneregy electron diffraction, revealing a statistical surface roughness for $T_{an}<600$ K and the formation of large terraces separated by monatomic steps for $600\ \mathrm{K}<T_{an}<800$ K. Annealing above ≈ 800 K results in step bunching, followed by a breakup of the film for $T_{an}>1000$ K. Both the extension of the AFM phase in the film and the annealing-induced changes of the surface topography can be explained by assuming the presence of a reconstructed Tb monolayer at the film-substrate interface that serves as an effective substrate on which a slightly strained Tb film lattice is stabilized upon annealing.

DOI: 10.1103/PhysRevB.72.035417 PACS number(s): 68.35.−p, 68.37.−d, 68.55.−a, 81.15.−z

I. INTRODUCTION

Most of the heavy rare-earth (RE) metals crystallize in an hcp-like structure, and their localized 4f magnetic moments order in a helical antiferromagnetic (AFM) phase upon cooling before they undergo a phase transition to ferromagnetic (FM) order.[1] In the helical AFM phase of the bulk metals Tb and Dy, the 4f moments form a spiral with all moments in an hcp-lattice basal plane pointing into a common in-plane direction that rotates as one proceeds along the crystallographic c axis.[2] The first-order phase transition from FM to AFM order at T_C is driven by a strong *magnetoelastic coupling* particularly between the orbital part of the 4f moments and the crystal lattice;[3] it is accompanied by a considerable lattice expansion along the easy axis of magnetization (b axis in Tb, a axis in Dy).[2] Consequently, it is affected when the lattice is strained by external forces: compressive (tensile) lattice strain decreases (increases) the Curie temperature T_C of *bulk* Tb thereby stabilizing (destabilizing) the AFM phase.[4–6]

Very large lattice strains are easily reached in heteroepitaxial film growth. Such *epitaxial strains* have been investigated extensively in RE "superlattices," in which layers of two different RE elements—a few atomic lattice planes each—are repeatedly (n times) grown on top of each other.[7] For $[\mathrm{Dy/Lu}]_n$ superlattices, a substantially increased T_C (destabilized AFM phase) has been observed,[8] while the opposite (stabilized AFM phase) was found for $[\mathrm{Dy/Y}]_n$[9] and superlattices constructed of other rare-earth elements.[10,11] Although this behavior follows the general trend that larger (smaller) c-axis lattice parameters go hand in hand with a destabilized (stabilized) AFM phase, one may question whether the observed changes of T_C can be attributed to epitaxial strain alone. This is because "nonmagnetic" spacer layers (Y, Lu) can affect the superlattice magnetic properties not only by epitaxial strain but also by their valence-band susceptibility.[12] It is well known that yttrium stabilizes the helical AFM order in binary RE *alloys* through valence-band hybridization,[13] and it has been observed that a capping layer of yttrium can strongly modify the exchange coupling strength of an epitaxial RE film.[14] Given that in superlattices both the magnetic layers and the spacer layers are rather thin (typically a few to several lattice planes), one is led to anticipate that the nonmagnetic (Y, Lu) spacer layers contribute significantly to the stability of the helical phase through their valence-band susceptibility. This view is corroborated by the strikingly large magnetic coherence length in $[\mathrm{Dy/Y}]_n$ and other RE superlattices in which helimagnetic order propagates across 10 nm thick nonmagnetic spacer layers without loss of phase.[15]

In a comprehensive investigation, Tsui and Flynn sandwiched 5 nm thick Dy(0001) films between $\mathrm{Y}_x\mathrm{Lu}_{1-x}$ alloy films of various stoichiometries.[16] When the adjacent alloy films had the in-plane lattice parameter of bulk Dy, the Dy films showed the same T_C as bulk Dy. This finding is rather surprising as one would expect a stabilized AFM phase (a lower T_C) when the Dy lattice is "epitaxially clamped" by the adjacent alloy films, i.e., when it is hindered to assume the tetragonal lattice distortion that is believed to "drive" the phase transition in bulk Dy.[16] Another study revealed a drastically lowered phase transition temperature ($T_C\approx 160$ K) of a 4 nm Tb(0001) film sandwiched between Y(0001) films.[17] However, in both studies the adjacent films were RE metal films of high valence-band susceptibility, just as in the mentioned superlattices so that an influence of the yttrium susceptibility on the AFM phase stability cannot be ruled out.

In order to identify the role of epitaxial strain in stabilizing the AFM phase in rare-earth metals, it should be informative to study single epitaxial films. The optimum thickness for obtaining a significant epitaxial strain in a metal film

is in the nanometer range,[7] well above a few atomic lattice planes, which helps to avoid that valence-band hybridization plays an important role, but still thin enough to prevent that the epitaxial strain relaxes across the film. Although there are numerous studies of rare-earth metal films grown on single-crystal substrates,[18–27] only a few of them have been concerned with the AFM phase stability.[16,17,28,29]

In this work we present the results of an investigation of the stability of the helical AFM phase of Tb(0001) films grown epitaxially on W(110). In contrast to previous studies, where mostly Y or RE alloys were used as templates and/or as capping layers, tungsten was chosen as substrate material because of its small magnetic susceptibility. Hence, the influence of the substrate valence-band structure on the magnetic properties of the Tb film can be neglected, and epitaxial strain is expected to be the dominant effect.

The paper is organized as follows: After a brief description of the sample preparation and experimental procedures in Sec. II, we present ac-susceptibility data and their analysis in Sec. III. The annealing-induced changes of the Tb film topography are described in Sec. IV, followed by a discussion in Sec. V. A summary and a brief outlook are given in Sec. VI.

II. EXPERIMENTAL

Tb(0001) films of 10 nm thickness were deposited on a W(110) single crystal (8 mm diam) in UHV (low 10^{-11} mbar range) at a rate of ≈ 2 atomic layers per minute. Details of substrate and film preparation have been described in Refs. 30 and 31. The film quality was checked *in situ* by low-energy electron diffraction (LEED), using standard back-view LEED optics. The magnetic ac susceptibility was measured by applying an oscillating magnetic field[32] of 57 Hz and 13 Oe amplitude along the *b* direction of the sample (easy axis of magnetization in bulk Tb),[2] which is parallel to the $[1\bar{1}0]$ direction in the W(110) surface plane (Nishiyama-Wassermann growth orientation).[33]

The magnetic ac-susceptibility was observed using the magneto-optical Kerr effect (MOKE) at $\lambda = 630$ nm.[34] With a visible-light penetration depth of ≈ 20 nm, the MOKE signal reflects the average susceptibility across the entire 10 nm thick Tb film. The signal was recorded while cooling the sample at a rate of 1 K/s. After each measurement, the sample was step-annealed for 60 s each at successively higher annealing temperatures T_{an}. Annealing was done without moving the sample so that all susceptibility curves were recorded from the same sample spot (illuminated area was ≈ 1 mm^2). The error bars of the given T_{an} are estimated to be ± 5 K, although, the relative uncertainty in comparing different susceptibility curves is better than ± 0.5 K. In order to ensure sample cleanness, in particular, after high-temperature annealing, we recorded complementary vacuum ultraviolet (VUV) photoemission spectra; they show a considerable uptake in W-4f line intensity upon "breakup" of the film, but no indication of contamination (no photoemission line intensity at 6 eV binding energy).

The LEED patterns were recorded *in situ*. The scanning tunneling microscope (STM) images were taken in the constant-current mode with an instrument designed for growth studies and described elsewhere[35] under the same conditions, in particular, using the same Tb evaporator.[31] The STM data were plane-fitted on atomically flat terraces to correct the tilt of the sample. In order to enhance the contrast, we mixed the tip height z and its derivative with respect to the fast scan direction x (i.e., dz/dx). This image processing suggests the spectator a topography that is illuminated by an invisible light source from the left.

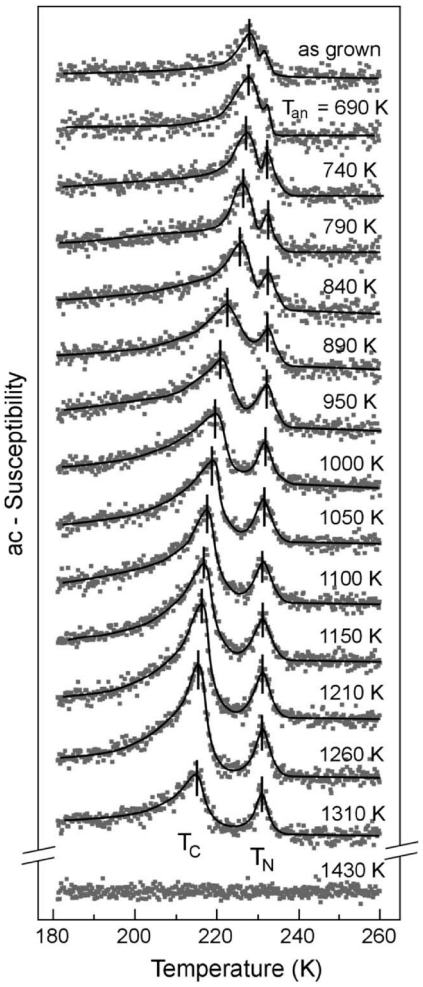

FIG. 1. ac-susceptibility vs temperature curves of 10 nm Tb(0001) films on W(110), annealed at successively higher temperatures, T_{an}. The curves were recorded during sample cool-down at a rate of 1 K/s, using an oscillating field of 13 Oe (amplitude) and 57 Hz. Vertical bars mark the T_C and T_N peak positions. The solid curves through the data points serve as a guide to the eyes.

III. MAGNETIC AC-SUSCEPTIBILITY

Figure 1 presents ac-susceptibility curves of a Tb film on W(110) deposited at room temperature and step-annealed at increasing temperatures T_{an} from 690 to 1430 K. The as-grown film shows a broad susceptibility structure peaking around 229 K, with a weak shoulder at higher temperatures. Upon annealing at 690 K, this shoulder grows, developing at $T_{an} = 740$ K into an independent peak. The two ac-

susceptibility peaks are well known from studies of bulk Tb single crystals.[36,37] According to these earlier studies the less intense peak around 232 K reflects the second-order phase transition from paramagnetic to helical AFM order (Neél temperature T_N), whereas the dominant peak at lower temperatures is associated with the first-order phase transition from helical AFM to FM order. The positions of the ac-susceptibility peaks serve as approximate measures of the phase-transition temperatures.[38]

As shown in Fig. 1 the T_C-peak intensity of the Tb film rises with increasing T_{an}, while the peak position shifts to lower temperatures. By contrast, position and intensity of the T_N peak remain rather stationary for all T_{an}. When annealing the film at $T_{an} > 1200$ K, the intensity of the T_C peak decreases readily, until it disappears completely for $T_{an} \geqslant 1430$ K. There are two possible reasons. As one has to conclude from TDS data in Ref. 39, that at this high temperature, less than a monolayer of Tb coverage remains on the surface. From the absence of valence-band exchange splitting of a monolayer of Gd/W(110),[40] one can expect that there is no (long-range) magnetic order of a (sub-) monolayer of Tb/W(110) as well. Therefore, although the vanishing susceptibility signal after annealing at 1430 K may result from complete desorption of Tb, it would also be in agreement with a remaining nonferromagnetic (sub-) monolayer.

The most important features of the ac-susceptibility data in Fig. 1 are highlighted in Fig. 2. Figure 2(a) shows that the position of the T_N peak in fact reduces slightly with increasing T_{an} at a slope of $\Delta T_N/\Delta T_{an} = -0.3$ K/100 K. By contrast, T_C reduces more steeply by $\Delta T_C/\Delta T_{an} = -1.0$ K/100 K in the annealing-temperature range up to ~850 K.[41] We shall refer to this region as region I. For higher T_{an}, there is a remarkable change in slope to $\Delta T_C/\Delta T_{an} \approx -2$ K/100 K. The height of the T_C peak, displayed in Fig. 2(b), increases significantly in region I, but remains rather stationary in region II up to $T_{an} \approx 950$ K. Yet, it rapidly increases with further annealing (region III), when it reaches its maximum at $T_{an} \approx 1200$ K. Above this temperature (region IV), the height of the T_C peak drops abruptly at $T_{an} \approx 1300$ K below 60% of its maximum value. Figure 2(c) shows the *width* [full width at half maximum (FWHM)] of both susceptibility peaks. The width of the T_N peak remains rather stationary at about 4.5 K for all annealing temperatures. It is broader than the width (≈3 K) reported for bulk Tb single crystals,[36,42] probably because of the higher oscillating-field amplitude used in the present experiments. The width of the T_C peak, by contrast, changes drastically with annealing temperature. Although it is nearly constant (≈7.5 K) in region I, it doubles at the border between regions II and III (reaching ≈15 K), before it drops again. (This probably indicates an inhomogeneous broadening due to a distribution of spatially varying lattice strain, see discussion below.) In region IV, the width of the T_C peak gets similarly small again as in region I(≈10 K).

The widths of the T_C peaks measured for the present Tb films are comparable to those of bulk Tb single crystals, and they have similarly asymmetric line profiles.[36,42] The asymmetry has been attributed to the rather complex temperature dependence of domain wall motion in the ac field in the FM regime.[41] Furthermore, the phase transition from helical AFM to FM order in very thick (≈700 nm) Tb films has been found to involve a formation of FM "blocks" some 15 K below but not above T_C;[43] this asymmetric behavior may contribute to the observed T_C-peak shape.

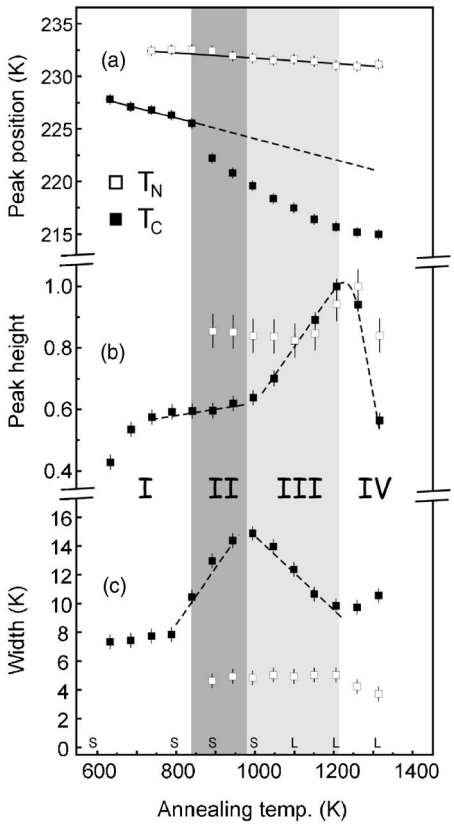

FIG. 2. Results of an analysis of the T_N and T_C peaks of the ac-susceptibility data shown in Fig. 1. (a) Peak positions, (b) relative peak heights, and (c) peak widths (FWHM). The solid lines are the results of linear fits to the data; dashed lines and the dashed curve in (b) serve as a guide to the eyes; for details, see text. The annealing temperatures employed for the STM images in Fig. 3 and for the LEED images in Fig. 4 are indicated on the abscissa by the letters *S* and *L*, respectively.

IV. TB-FILM SURFACE TOPOGRAPHY

In the present work we chose standard UHV techniques, such as LEED and room-temperature STM, to monitor the annealing-induced changes of the surface topography of the Tb film.

A. STM images

Figure 3 shows STM images of 10 nm Tb(0001) films deposited at 300 K on W(110), upon annealing at various temperatures ranging from $T_{an} = 580$–1000 K. For comparison to the susceptibility data, the annealing temperatures are marked by *S* on the abscissa of Fig. 2. The top row of Fig. 3 shows the film surface upon annealing at 580 K; it has hardly changed from the as-grown state (not shown). The Tb film surface consists of islands of varying size, with lateral diam-

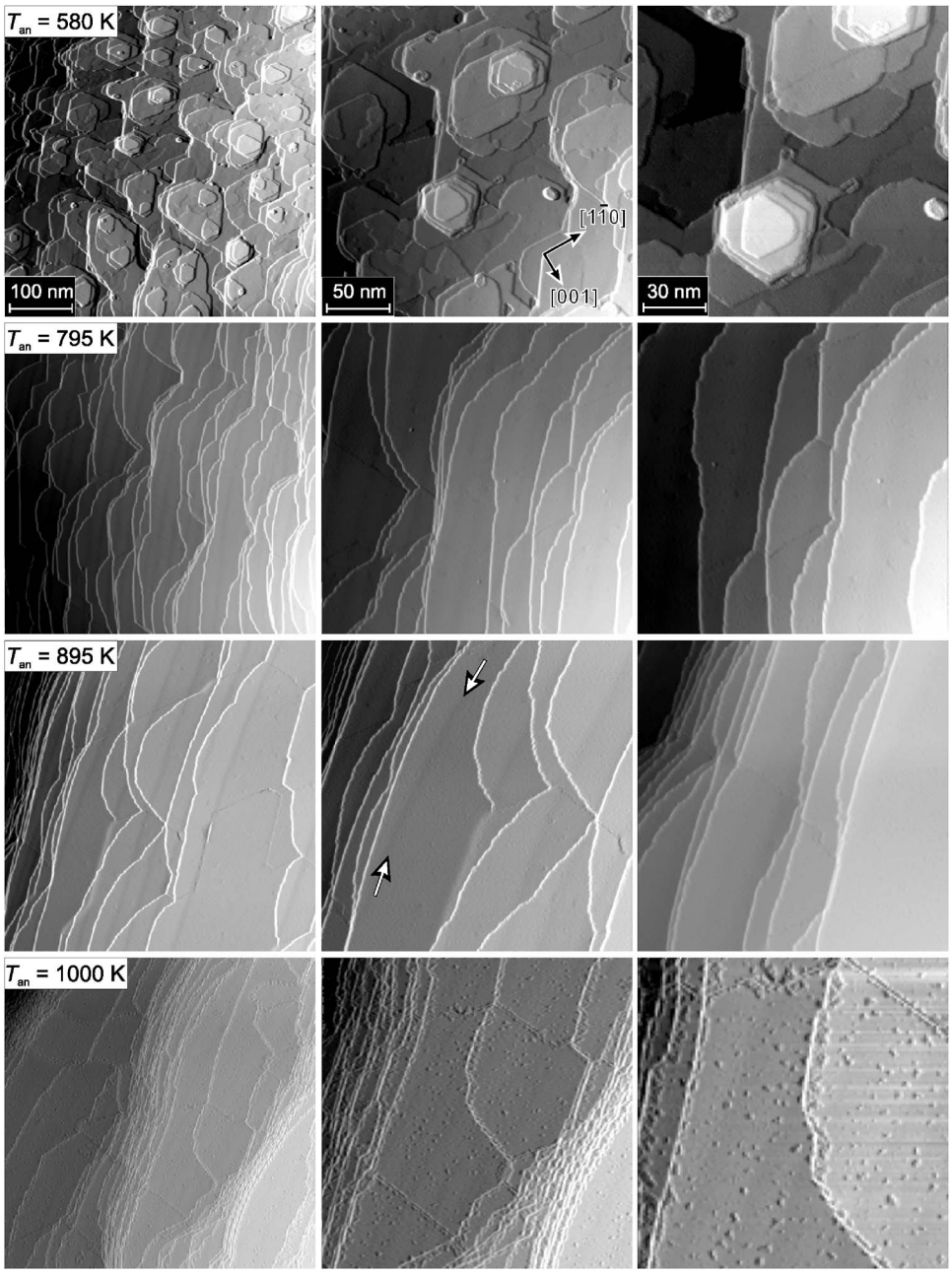

FIG. 3. STM topographs of 10 nm Tb(0001) films on W(110), recorded at room temperature upon annealing at $T_{an}=580$ K (top row), $T_{an}=795$ K (second row), $T_{an}=895$ K (third row), and $T_{an}=1000$ K (bottom row) at three different magnifications (columns). The orientation of the W(110) substrate is indicated by black arrows (top row); it is identical for all images. The surface steps of the Tb film follow the monoatomic steps of the substrate surface that are weakly visible as smeared steps (white arrows in third row).

eters mostly between 30 and 50 nm. The steps are monatomic, and the island shapes clearly reveal the threefold symmetry of the close-packed surface in [0001] crystal direction.

The islands disappear upon annealing at 795 K (second row of Fig. 3). The entire film surface now consists of terraces of some 30 nm average width, separated by monoatomic steps. The change from islands to flat terraces indicates that, upon annealing at $T_{an}=795$ K, there is sufficient mobility of Tb surface-layer atoms to diffuse to adsorption sites of higher coordination number (lower step edges). In this way small islands disappear, resulting in an effective reduction of the surface roughness.

Increasing the annealing temperature by 100 K to $T_{an}=895$ K (third row of Fig. 3) induces "bunching" of monatomic steps between terraces, which is most clearly discernible on the left side of the overview image (left column). The surface steps of the film do not coincide with any particular high-symmetry direction of the W(110) substrate, which are indicated by black arrows in the top row. Yet, they run, by and large, parallel to the substrate surface steps, which—upon closer inspection—become visible as lines (indicated in the third row of Fig. 3 by arrows).

Step bunching becomes even more pronounced upon annealing at $T_{an}=1000$ K (bottom row), accompanied by an inevitable formation of wider terraces, some being as wide as 100 nm. The stained surface images in the bottom row of Fig. 3 reflect technical difficulties in reaching 1000 K in the STM chamber; because of degassing from the sample holder at this high annealing temperature, the Tb surface state is quenched locally.[44] This problem prohibited annealing at even higher T_{an}.

B. LEED images

To check if the topography of the Tb film undergoes further significant changes upon annealing above 1000 K, we recorded LEED images, a selection of which are shown in Fig. 4. The annealing temperatures are marked by *L* on the abscissa of Fig. 2. The image in Fig. 4(a) corresponds to the surface upon annealing at $T_{an}=1100$ K. It shows a plain (1×1) pattern that is characteristic of a close-packed crystal surface. In the whole temperature range T_{an} between 800 and 1000 K the LEED patterns remain purely hexagonal (images not shown here). Although the LEED pattern in Fig. 4(a) seems to reflect a well-ordered smooth film, one cannot strictly exclude—from the LEED pattern alone—that the metastable Tb film has already begun to break up at this annealing temperature (1100 K).[45] It is rather likely that the process of step bunching, which is observed by STM upon annealing at $T_{an}=895$ K and which gets more pronounced for $T_{an}=1000$ K, progresses with higher T_{an} and that it will eventually lead to the formation of deep notches in the film.

The LEED image in Fig. 4(b) was recorded after annealing the film at 1210 K, right at the maximum of the ac-susceptibility T_C peak height. Faint satellite LEED spots appear around the main peaks, best visible near the lower- and upper-right main peaks. If annealed at 100 K higher temperature (of $T_{an}=1310$ K), i.e., at the annealing temperature where the T_C-peak height is greatly reduced [cf. Fig. 2(b)], satellite "rings" around each main hexagonal spot become clearly visible, cf. Fig. 4(c). Their appearance indicates that electrons are scattered from the Tb film as well as from the W substrate. At the LEED energy of 150 eV used here, the electron mean-free path is as short as a few crystal lattice planes; hence, there must be regions where the film has become as thin as a few lattice planes. Note that the satellite LEED pattern in Fig. 4(c) resembles the one of Gd/W(110) in the *monolayer coverage* regime.[46] One may thus conclude that, upon annealing at 1310 K, the present Tb film contains deep notches. Very similar LEED patterns were observed by Tober *et al.* in the case of "over-annealed" Gd(0001)/W(110) films that were broken up into islands, with wide areas of monolayer coverage in between.[47]

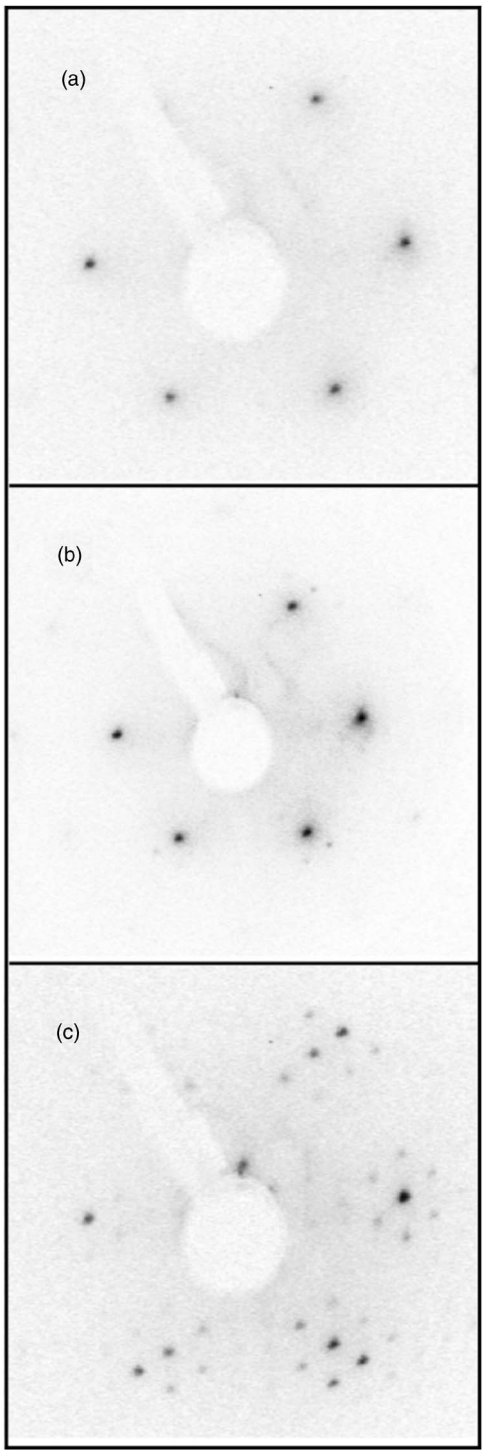

FIG. 4. LEED images (inverted contrast) of 10 nm Tb(0001) films on W(110) recorded with an 150 eV electron beam at room temperature upon annealing at (a) $T_{an}=1100$ K, (b) $T_{an}=1210$ K, and (c) $T_{an}=1310$ K. The characteristic hexagonal pattern of a close-packed (0001) surface in (a) was also found for $T_{an}<1100$ K. (b) Weak satellite LEED intensity becomes only visible upon high annealing at $T_{an}=1210$ K; (c) the satellite intensity increases for higher T_{an}. Center and upper left corner of the images are masked by the electron-gun holder.

V. DISCUSSION

The key experimental finding of the present work, displayed in Figs. 1 and 2, concerns the separation between the T_N and T_C susceptibility peaks. It increases from $T_N-T_C=\Delta T_{N,C}\approx5$ K (for $T_{an}=740$ K, where the peaks have clearly separated) to a maximum value of $\Delta T_{N,C}=17$ K (for $T_{an}=1210$ K). This is significantly larger than the interval of helical AFM order of unstrained *bulk* Tb single crystals, for which values up to 10.8 K have been reported.[36]

In order to understand the annealing-induced extension of the helical AFM phase, we compare to bulk Tb single crystals for which $\Delta T_{N,C}$ was found to extend (reduce) upon compressive (tensile) lattice strain.[4–6] This behavior has been attributed to the large *magneto-elastic coupling* that drives the first-order phase transition in all heavy RE metals with a nonspherical 4f-charge distribution. The doughnut-shaped 4f

charge cloud of trivalent Tb ions ($4f^8$ configuration) gives rise to a particularly strong interaction between the orbital part of the 4f magnetic moment and the crystal lattice. While in the undistorted close-packed crystal lattice, the helical magnetic order is favored through the Tb valence-band susceptibility,[1] the total energy of the system is significantly reduced through the tetragonal lattice distortion in the FM phase below T_C, in which the Tb lattice is elongated along the easy axis of magnetization, the hcp *b* axis.[48] Therefore, a reduction of the *b* lattice parameter through external forces ("forced magnetostriction") should stabilize the AFM phase. Moreover, based on strain experiments with bulk Tb crystals, Andrianov *et al.*[6] have suggested that there is a critical *c*/*a* ratio below which no stable AFM phase can exist. Indeed, x-ray-diffraction data[49] give a ratio (c/a)=1.581 for bulk Tb and the fact that this value is just below the proposed critical ratio (1.582) is held responsible for the rather low stability (i.e., narrow temperature range) of AFM order in bulk Tb crystals.[6]

In light of the close relationship between AFM phase stability and lattice parameters, it would be worthwhile to measure possible changes of the Tb film lattice constants *in situ* during annealing. Although surface x-ray-diffraction experiments have become feasible,[50] such an experiment would be quite cumbersome given the vacuum requirements for preparation and *in situ* analysis of the RE metal films.[31]

To our knowledge there have been no investigations of annealing-induced changes of the crystal structure of a RE metal film. In the following we present arguments that lead one to assume the existence of a *reconstructed* Tb atomic layer right at the film-substrate interface. (i) Owing to the vastly different cohesive energies of Tb metal and the W(110) refractory-metal substrate[51] the Tb-W bonds "across" the interface are much stronger than the Tb-Tb bonds. This has been shown experimentally by thermal desorption studies (TDS) of Tb/W(110) (in the film thickness regime around one monolayer) revealing a much higher desorption energy for Tb atoms of the interface layer than for second-layer Tb atoms.[39] Hence, the Tb-W bonds should be decisive for the interface crystal structure. (ii) LEED and STM studies of (sub-) monolayer coverages of Gd and Tb on W(110) have revealed that the monolayer on W(110) is reconstructed.[39,47,52] From the almost identical cohesive energies of bulk Gd and Tb one expects the same qualitative behavior for the two elements.[39,52] Although there is some debate regarding details,[53] all studies agree that the monolayer on W(110) is reconstructed, hereby reducing the RE metal lattice strain to some 1%.[54,55] (iii) The presence of a reconstructed monolayer at the Tb/W(110) interface is also expected from the model for heteroepitaxial film growth by J. van der Merwe.[56,57] According to the model, there is a maximum interface layer strain of typically ≈9%, above which the elastic energy becomes too large for pseudomorphic growth, which means that the large misfit of 12% between Tb (in-plane lattice constant 360.5 pm) and W (316.5 pm) inevitably results in a reconstruction of the Tb interface layer.[57]

All studies so far have been restricted to the (sub-) monolayer coverage regime, and at the time of writing there is no experimental proof that a reconstructed Tb/W(110) interface layer also exists in thick films. Yet, based on the energy arguments given above, we assume that a reconstructed Tb interface layer is present also in the 10 nm thick Tb films on W(110). The reconstructed and strongly bound Tb interface layer serves as an effective substrate Tb-monolayer/W(110) for the Tb film.

We now address the question how far a small in-plane lattice strain of the order of 1% can extend into the Tb film. According to the van der Merwe model,[56] in-plane film strains below ≈3% reduce exponentially with distance *z* from the interface with the characteristic relaxation length z_0. z_0 scales with the average lateral separation *p* of dislocations, so that the strain extends some $\frac{1}{2}p$ into the film.[56] Applying the model to Tb on W(110), we expect that an in-plane lattice strain of the order of 1% reaches as far as 100 nm, i.e., an order of magnitude further than the film thickness; hence the strain should be roughly constant over the entire film. However, the growth model only applies to systems in thermal equilibrium. This condition is certainly not met by the as-grown and gently annealed Tb films (top row of Fig. 3), but more so by the films annealed at higher temperatures (third and bottom row of Fig. 3). Therefore, we expect that the predictions of the growth model, i.e., a reconstructed Tb interface layer with small in-plane lattice strain and a very "slow" strain relaxation over the Tb film, apply best to the high-annealed films in region III. The LEED images in Figs. 4(a) and 4(b) reveal clear hexagonal patterns in region III with only faint satellite intensity at the high-temperature end. Intense LEED satellites appear only in Fig. 4(c) indicating that the film breaks up into islands (and largely desorbs) in region IV.

The atomic mobility in annealing temperature region III leads to a low defect concentration (susceptibility shows most narrow and most intense T_C peak) and step bunching with wide terraces (STM) at the film surface; in this state of annealing the Tb film apparently is subject to a rather homogeneous epitaxial lattice strain. (The strain is on the order of 1% since the lattice mismatch between W and Tb is largely accommodated by the reconstructed interface.) It is the *simultaneous appearance* of step bunching and the extended temperature range of the AFM phase (cf. Fig. 2) which suggests that the enhancement of the AFM phase stability is owing to the epitaxial lattice strain. Note that the twofold symmetry of the W(110) substrate is likely to induce an uniaxial in-plane lattice strain, i.e., a tetragonal distortion of the film lattice from hexagonal to orthorhombic symmetry (γ mode[58]); hence, the observed extension of the AFM temperature range upon annealing points towards a *reduced b*-lattice parameter in the epitaxially strained Tb film that stabilizes the AFM phase through "forced magnetostriction." Yet this hypothesis awaits future experimental verification.

VI. SUMMARY AND OUTLOOK

Magnetic ac-susceptibility data of high-annealed Tb(0001) metal films on W(110) show a wider temperature range of the AFM phase ($\Delta T_{N,C}=17$ K) than bulk Tb single crystals. On the basis of the annealing-induced changes of the film surface topography observed via STM and LEED we

arrive at the following interpretation of the susceptibility data, cf. Figs. 1 and 2:

Region I ($T_{an} < 840$ K): The film quality improves with increasing T_{an} until there is sufficient surface atom mobility to form an atomically flat film surface with 30.50 nm wide terraces (separated by monoatomic steps). ac-susceptibility data reveal minor changes.

Region II ($840\ \text{K} < T_{an} < 980$ K): An enhanced film lattice defect mobility allows the formation of a reconstructed Tb atomic layer at the Tb-W interface owing to the high Tb-W cohesive energy, forming an effective substrate on top of which the Tb film is stabilized with a lattice strain of some 1%. The strain is likely to cause the observed extension of the temperature range of the AFM phase (enhanced AFM phase stability), that is revealed by the substantial reduction of T_C with increasing annealing temperature.

Region III ($980\ \text{K} < T_{an} < 1210$ K): With a very high defect mobility at the rather high T_{an} the film lattice approaches thermodynamic equilibrium. The pronounced step bunching, accompanied by the formation of very wide terraces, leads to maximum epitaxial film strain, which further stabilizes the AFM phase (maximum AFM temperature range, $T_{N,C} = 17$ K). Concomitantly, a minimum defect concentration is reached when T_{an} approaches the upper bound of region III, where the susceptibility T_C peak has increased by 50% in height and has sharpened considerably (−30%).

Region IV ($1210\ \text{K} < T_{an}$): The film desorbs (T_C-peak height −40%) with no significant change in lattice strain (stationary T_C).

From the strongly different Tb-W and Tb-Tb cohesive energies, and in agreement with the van der Merve model for heteroepitaxial film growth, we expect that a reconstructed Tb interface layer forms upon annealing, even in the 10 nm thick film. According to the growth model, a small in-plane strain of some 1% of the Tb interface layer can be adopted by the neighboring lattice planes; the strain thus hardly decays over the film thickness resulting in an approximately homogeneous strain across the entire film.

We suggest *in situ* x-ray-scattering experiments on epitaxial films of Tb and other RE metals[59,60] in order to (i) investigate the annealing-induced changes of lattice parameters in heteroepitaxial film growth and (ii) experimentally verify the expected reconstruction at the film-substrate interface.

ACKNOWLEDGMENTS

This work was supported by the Deutsche Forschungsgemeinschaft, SFB 290 (TP A6). J. E. Prieto thanks the Alexander-von-Humboldt Stiftung for financial support.

*Present address: University of Western Ontario, London, ON, Canada

†Corresponding author. Electronic address: starke@physik.fu-berlin.de

[1] S. Legvold, in *Ferromagnetic Materials*, edited by E. P. Wohlfarth (Elsevier, Amsterdam, 1980), vol. 1, p. 183.

[2] J. J. Rhyne, in *Rare Earth Magnetism*, edited by R. J. Elliott (Plenum, London, 1972), pp. 129–185.

[3] K. A. McEwen, in *Handbook on the Physics and Chemistry of Rare Earths*, edited by K. A. Gschneidner and L. Eyring (Elsevier, Amsterdam, 1978), vol. 1, pp. 411–488.

[4] A. M. Tishin, Y. I. Spichkin, and J. Bohr, in *Handbook on the Physics and Chemistry of Rare Earths*, edited by K. Gschneidner and L. Eyring (Elsevier, Amsterdam, 1999), vol. 26, pp. 88–176.

[5] A. V. Andrianov, J. Magn. Magn. Mater. **196-197**, 714 (1999).

[6] A. V. Andrianov, D. I. Kosarev, and A. I. Beskrovnyi, Phys. Rev. B **62**, 13844 (2000).

[7] C. P. Flynn and M. B. Salamon, in *Handbook on the Physics and Chemistry of Rare Earths*, edited by K. A. Gschneidner and L. Eyring (Elsevier, Amsterdam, 1996), vol. 22, p. 1.

[8] R. S. Beach, J. A. Borchers, A. Matheny, R. W. Erwin, M. B. Salamon, B. Everitt, K. Pettit, J. J. Rhyne, and C. P. Flynn, Phys. Rev. Lett. **70**, 3502 (1993).

[9] R. W. Erwin, J. J. Rhyne, M. B. Salamon, J. Borchers, S. Sinha, R. Du, J. E. Cunningham, and C. P. Flynn, Phys. Rev. B **35**, 6808 (1987).

[10] D. A. Jehan, D. F. McMorrow, R. A. Cowley, R. C. C. Ward, M. R. Wells, N. Hagmann, and K. N. Clausen, Phys. Rev. B **48**, 5594 (1993).

[11] J. A. Borchers, M. B. Salamon, R. W. Erwin, J. J. Rhyne, R. R. Du, and C. P. Flynn, Phys. Rev. B **43**, 3123 (1991).

[12] S. B. Dugdale, H. M. Fretwell, M. A. Alam, G. Kontrym-Sznajd, R. N. West, and S. Badrzadeh, Phys. Rev. Lett. **79**, 941 (1997).

[13] H. M. Fretwell, S. B. Dugdale, M. A. Alam, D. C. R. Hedley, A. Rodriguez-Gonzalez, and S. B. Palmer, Phys. Rev. Lett. **82**, 3867 (1999).

[14] H. Yamazaki, Y. Tanaka, and K. Katsumata, J. Magn. Magn. Mater. **198**, 279 (1999).

[15] J. J. Rhyne, J. A. Borchers, R. R. Du, R. W. Erwin, C. P. Flynn, and M. B. Salamon, J. Less-Common Met. **148**, 17 (1989).

[16] F. Tsui and C. P. Flynn, Phys. Rev. Lett. **71**, 1462 (1993).

[17] C. Dufour, K. Dumesnil, A. Mougin, P. Mangin, and M. Hennion, J. Phys.: Condens. Matter **11**, L497 (1999).

[18] U. Stetter, M. Farle, K. Baberschke, and W. G. Clarke, Phys. Rev. B **45**, R503 (1992).

[19] G. A. Mulhollan, K. Garrison, and J. L. Erskine, Phys. Rev. Lett. **69**, 3240 (1992).

[20] H. Tang, D. Weller, T. G. Walker, J. C. Scott, C. Chappert, H. Hopster, A. W. Pang, D. S. Dessau, and D. P. Pappas, Phys. Rev. Lett. **71**, 444 (1993).

[21] M. Farle, W. A. Lewis, and K. Baberschke, Appl. Phys. Lett. **62**, 2728 (1993).

[22] U. Paschen, C. Sürgers, and H. v. Löhneysen, Z. Phys. B: Condens. Matter **90**, 289 (1993).

[23] A. Berger, A. W. Pang, and H. Hopster, J. Magn. Magn. Mater. **137**, L1 (1994).

[24] M. Farle and W. Lewis, J. Appl. Phys. **75**, 5605 (1994).

[25] K. Starke, E. Navas, E. Arenholz, Z. Hu, L. Baumgarten, G. van der Laan, C. T. Chen, and G. Kaindl, Phys. Rev. B **55**, 2672 (1997).

[26] M. Bode, M. Getzlaff, and R. Wiesendanger, Phys. Rev. Lett. **81**, 4256 (1998).
[27] E. D. Tober, F. J. Palomares, R. X. Ynzunza, R. Denecke, J. Morais, Z. Wang, G. Bino, J. Liesegang, Z. Hussain, and C. S. Fadley, Phys. Rev. Lett. **81**, 2360 (1998).
[28] R. S. Beach, J. A. Borchers, R. W. Erwin, J. J. Rhyne, A. Matheny, C. P. Flynn, and M. B. Salamon, J. Appl. Phys. **69**, 4535 (1991).
[29] H. Yamazaki, Y. Tanaka, and K. Katsumata, J. Phys.: Condens. Matter **10**, L283 (1998).
[30] E. Navas, K. Starke, C. Laubschat, E. Weschke, and G. Kaindl, Phys. Rev. B **48**, R14753 (1993).
[31] K. Starke, *Magnetic Dichroism in Core-level Photoemission* (Springer, Berlin, 2000).
[32] F. Heigl, O. Krupin, G. Kaindl, and K. Starke, Rev. Sci. Instrum. **73**, 369 (2002).
[33] H. Li, D. Tian, J. Quinn, Y. S. Li, S. C. Wu, and F. Jona, Phys. Rev. B **45**, 3853 (1992).
[34] Z. Q. Qiu and S. D. Bader, Rev. Sci. Instrum. **71**, 1243 (2000).
[35] C. Witt, U. Mick, and M. B. R. Wiesendanger, Rev. Sci. Instrum. **68**, 1455 (1997).
[36] A. del Moral and E. W. Lee, J. Phys. F: Met. Phys. **4**, 280 (1974).
[37] T. J. McKenna, S. J. Campbell, D. H. Chaplin, and G. V. H. Wilson, J. Magn. Magn. Mater. **104-107**, 1505 (1992).
[38] It was shown for ferromagnetic Ni that the experimental peak position is a lower bound of the true T_C, but deviations between the experimental susceptibility peak and T_C are on the order of $T/T_C \approx 10^{-3}$ and can be neglected here (Ref. 61).
[39] J. Kołaczkiewicz and E. Bauer, Surf. Sci. **175**, 487 (1986).
[40] M. Getzlaff *et al.*, J. Magn. Magn. Mater. **184**, 155 (1998).
[41] The fact that the first-order phase transition temperature changes more steeply with annealing than T_N is reminiscent of the Tb bulk behavior. When tensile stress is applied along the *c* axis of a bulk Tb crystal, T_C undergoes much stronger changes with increasing stress than T_N ($\approx$6 K/kbar versus 0.9 K/kbar) (Ref. 6).
[42] T. J. McKenna, S. J. Campbell, D. H. Chaplin, and G. V. H. Wilson, J. Phys.: Condens. Matter **3**, 1855 (1991).
[43] Very thick (700 nm) epitaxial Tb films, grown on a Nb(110) film on a sapphire single crystal, exhibit the formation of ferromagnetic "blocks" over a range of a few 10 K before a single-domain FM phase is formed (Ref. 17).
[44] M. Getzlaff, M. Bode, R. Pascal, and R. Wiesendanger, Phys. Rev. B **59**, 8195 (1999).
[45] M. Farle, K. Baberschke, U. Stetter, A. Aspelmeier, and F. Gerhardter, Phys. Rev. B **47**, R11571 (1993).
[46] S. A. Nepijko, M. Getzlaff, R. Pascal, C. Zarnitz, M. Bode, and R. Wiesendanger, Surf. Sci. **466**, 89 (2000).
[47] E. D. Tober, R. X. Ynzunza, C. Westphal, and C. S. Fadley, Phys. Rev. B **53**, 5444 (1996).
[48] J. J. Rhyne and S. Legvold, Phys. Rev. **138**, A507 (1965).
[49] E. Preuss, B. Krahl-Urban, and R. Butz, *Laue Atlas* (Bertelsmann Universitätsverlag, Düsseldorf, 1974).
[50] H. L. Meyerheim, R. Popescu, J. Kirschner, N. Jedrecy, M. Sauvage-Simkin, B. Heinrich, and R. Pinchaux, Phys. Rev. Lett. **87**, 076102 (2001).
[51] *Elastic, Piezoelectric, Pyroelectric, Piezooptic, Electrooptic Constants, and Nonlinear Dielectric Susceptibilities of Crystals, Landolt-Börnstein*, Vol. III-11, edited by K.-H. Hellwege and A. M. Hellwege (Spinger, Berlin, 1979).
[52] R. Pascal, C. Zarnitz, H. Tödter, M. Bode, M. Getzlaff, and R. Wiesendanger, Appl. Phys. A **66**, S1121 (1998).
[53] A (14×7) reconstruction was proposed earlier for the Gd monolayer on W110 (Ref. 47), but a different one has been identified more recently (together with a small relaxation of the tungsten interface layer) (Ref. 46).
[54] This is much less than earlier assumptions of a strongly compressed first monolayer, J. Kołaczkiewicz and E. Bauer, Surf. Sci. **175**, 487 (1986).
[55] The growth of Gd and Tb in the submonolayer thickness range on W(110) is known to be almost identical, see Refs. 39 and 62.
[56] J. H. van der Merwe, Phys. Rev. **34**, 117 (1963).
[57] J. H. van der Merwe, Phys. Rev. **34**, 123 (1963).
[58] E. R. Callen and H. B. Callen, Phys. Rev. **139**, A455 (1965).
[59] E. Weschke, A. Y. Grigoriev, C. Schüßler-Langeheine, C. Mazumdar, R. Meier, S. Vandre, S. Ram, L. Kilian, G. Kaindl, and C. Sutter, Phys. Rev. Lett. **83**, 584 (1999).
[60] H. L. Meyerheim, D. Sander, R. Popescu, J. Kirschner, P. Steadman, and S. Ferrer, Phys. Rev. B **64**, 045414 (2001).
[61] U. Bovensiepen, C. Rüdt, P. Poulopoulos, and K. Babaerschke, J. Magn. Magn. Mater. **231**, 65 (2001).
[62] R. Pascal, C. Zarnitz, H. Tröder, M. Bode, M. Getzlaff, and R. Wiesendanger, Appl. Phys. A **66**, S1121 (1997).